# RANS Simulations of Chemical Reactions in Cooling Films

*G. Frank, F. Ferraro and M. Pfitzner*
*Institut für Thermodynamik (LRT10)*
*Universität der Bundeswehr München*
*Werner-Heisenberg-Weg 39, 85577 Neubiberg*

## Abstract

Film cooling in rocket and turbomachinery engines is used to protect combustion chamber walls from hot main stream gases and keep the wall temperature within the safety ranges. The possible occurrence of chemical reactions due to mixing of fuel and oxidizer in the cooling film near the wall can lead to high heat loads. New parameters to describe the cooling film are defined and numerical investigations to determine the influence of operating conditions on the additional heat loads are performed. Requirements on combustion models for further investigations on turbulent flows are identified.

## 1. Introduction

In the design of liquid rocket motors high combustion pressures (e.g. 19 MPa in the SSME) and temperatures are required to obtain good performance. With increasing pressure and temperature, the thermal loads to the chamber walls can become too high and cause failure or even melting of the material. Most of the chamber materials in fact lose strength and become weaker as the temperature increases [1]. Regenerative cooling and radiation cooling are the conventional cooling methods used to keep the wall temperature in the safety range. In the first technique the cooling is accomplished by high velocity fuel flowing in the cooling channels inside chamber walls. The walls are convectively cooled. In the second technique the heat is radiated away from the surface of the chamber walls. This is normally employed in the nozzle where the heat can be radiated to the environment. In the other parts of the engine a combination of these two methods is used.
For high performance engines these methods can be insufficient. In rocket combustion chambers film cooling is largely used as supplementary method to prevent high wall temperatures. A film of liquid or gaseous coolant is injected at low velocity through orifices along the inner surface of the combustion chamber to form a protective cooling film. Additionally the injectors near the wall can be designed in a way that a different air-fuel ratio near the wall is achieved and the combustion temperature near the wall is lower. Film cooling is also used in gas turbine engines. Here the air from the compressor is injected through a series of holes in the combustor wall or turbine blade surface. This allows turbines to operate at higher temperature increasing the efficiency of the engine [2].
The thickness of the coolant film decreases downstream the injection point because of the interaction with hot combustion products. When the main hot flow is mixed with the cooling film, chemical reactions can occur between residual oxidizer and the cooling fuel (rocket combustor) or between residual fuel and cooling air (gas turbine). This event can reduce drastically the cooling efficiency. Recent experimental [3, 4] and numerical studies [5] on turbomachinery applications show the increased heat load due to this effect. Liu et al. [6] presents an analytical model for reactive flow over a porous surface, where it is found that the flame temperature of a secondary reaction zone depends on temperature and composition of the two streams, but the flame location and heat flux are additionally functions of thermodynamic flow properties. Non reacting film cooling in rocket combustors was extensively investigated by Haidn [7, 8, 9, 10]. Experimental results for a subscale LOX/$CH_4$ combustion chamber are discussed and the efficiency of film cooling is evaluated. The accuracy of a numerical investigation depends on the near wall treatment of the CFD code, the species diffusion, the combustion model and the flame-wall interaction.
In this work the film cooling effectiveness and the occurrence of secondary reactions within the cooling layer are examined under different operation conditions. Methane and hydrogen film cooling are simulated varying hot gas temperature, initial composition and blowing ratio. The effects of the geometry is also evaluated modifying the slot height of the cooling film injection. Results by using one-step reaction and a laminar steady flamelet model obtained with detailed kinetics mechanisms are compared.

## 2. Film cooling

### 2.1 Film cooling parameters for incompressible, constant fluid properties flows

Film cooling is used to keep the wall temperature below some critical value. Therefore for a given mainstream temperature and an allowable wall heat transfer, the surface temperature with a given cooling film shall be predicted. The convective heat flux to the wall is described via

$$q = h \cdot (T_w - T_{ref}), \tag{1}$$

where $h$ is the convective heat transfer coefficient. The reference temperature $T_{ref}$ is normally chosen as the surface temperature of an adiabatic wall $T_{aw}$. For a non-film cooled wall this temperature would be equivalent to the free stream temperature $T_{aw} = T_\infty$ or the recovery temperature for high speed flows. The heat transfer coefficient $h$ depends primarily on the mainstream boundary layer flow, that means, for a film cooled geometry, $h$ is often found to be close to the value without film cooling [11]. The main goal is therefore the prediction of the adiabatic wall temperature $T_{aw}$. The adiabatic wall temperature is influenced by the film cooling geometry (e.g. slot injection, hole injection), the primary and secondary flow fields and the temperature difference between the gas streams. A conventionally used parameter to characterize the two flow fields is the blowing ratio

$$M = \frac{\rho_w \cdot u_w}{\rho_\infty \cdot u_\infty}, \tag{2}$$

where $\rho_\infty$ and $u_\infty$ are the density and velocity of the main stream and $\rho_w$ and $u_w$ are the density and velocity of the injected coolant. To evaluate the efficiency of the film cooling, independently of the operating temperatures, a film cooling effectiveness $\eta$ is defined as

$$\eta = \frac{T_{aw} - T_\infty}{T_2 - T_\infty}, \tag{3}$$

where $T_2$ represents the temperature of the cooling fluid.
In constant property flow the energy equation is linear in temperature and the temperature field and flow field are not coupled. The film cooling effectiveness depends only on geometry and on primary and secondary flows characterized by Reynolds, Prandtl and Mach numbers. The transport equation for any conserved scalar is analogous to the energy equation. This analogy can be exploited and when Lewis number is unity the film cooling effectiveness can be defined as

$$\eta^\star = \frac{Z_w - Z_\infty}{Z_2 - Z_\infty}, \tag{4}$$

where $Z$ can be a mass fraction or concentration of a tracer gas. This analogy is often used for experimental studies of film cooling, where an impermeable wall is easier to realize than an adiabatic wall.

### 2.2 Film cooling parameters for reacting boundary layer

With possible chemical reactions in the boundary layer, a source term is added to the energy equation, which becomes not linear in temperature. Therefore a definition of $\eta$ via temperatures (eq. (3)) is not useful anymore. The definition of $\eta^\star$ as a mixture fraction is still applicable to account for the mixing of cooling fluid with the main stream. The mixture fraction $Z$ is defined as

$$Z = 1 - \frac{\mathrm{N}_2(x)}{\mathrm{N}_{2inlet}}, \tag{5}$$

where $\mathrm{N}_2$ is the mass fraction of nitrogen. When equal diffusivity of the species is assumed ($Le = 1$) an inert species like nitrogen is transported as a conserved scalar and can be used to define the mixture fraction.
Another parameter to characterize the occurring chemical reactions needs to be defined. We propose here a temperature ratio using the adiabatic flame temperature, which is the thermodynamic upper limit to the magnitude of heat release, and $T_2$, which is the coolant temperature and lower temperature limit

$$\Theta = \frac{T(x) - T_2}{T_{ad.flame} - T_2}. \tag{6}$$

## 3. Set-up of numerical simulations

### 3.1 Geometry and mesh

A simple 2D-geometry is used to represent the flow over a flat plate and a slot injection of the cooling film. The domain is shown in figure 1; its size is 2 cm x 2 cm. The slot for the main configuration is chosen to be $s_0 = 0.25$ mm,

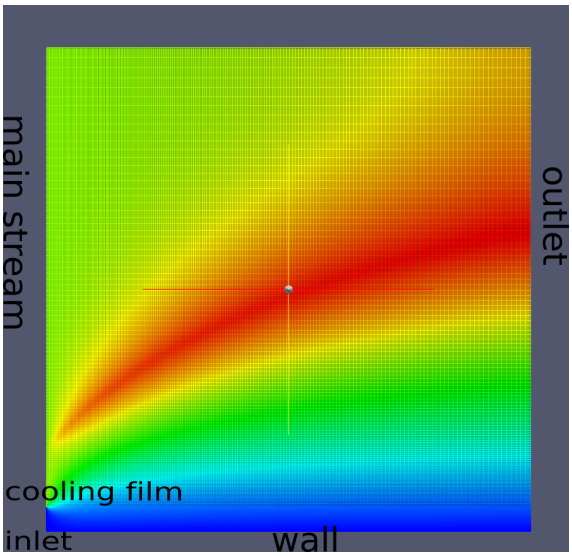


Figure 1: Investigated domain

a slot height which is used in experiments for film-cooling in a rocket combustion chamber [7]. The numerical domain extends therefore 80 slot heights downstream. The effects of the film cooling can be seen much further downstream, but due to computation time requirements and a desired good grid resolution this domain length is deemed sufficient. 200 x 165 = 33 000 gridpoints are used, with 15 grid points for the slot height. The points are clustered at the assumend position of the flame, i.e. in the shear layer between cooling film and main stream. The grid convergence was examined and the overall GCI [12] index was found to be around 1%, therefore the resolution is sufficient.
A cooled wall and the enthalpy loss affect the chemical reactions. To examine the effect of flame-wall distance the configuration is changed to bigger slot sizes of $s_1 = 0.5$ mm and $s_2 = 1$ mm, keeping the overall domain unchanged.

### 3.2 Boundary conditions

The simulations examine laminar film cooling, therefore the main flow velocity is set to $0.1\,\mathrm{m\,s^{-1}}$. The Reynolds number based on the domain length is $Re = 120$. The cooling film is either pure methane ($CH_4$) or pure hydrogen ($H_2$) at $T_2 = 300$ K. The wall is set either adiabatic or to a constant temperature of $T_w = 300$ K.
The reference set-up is a hot air flow with $T_\infty = 1800$ K and an inlet velocity for the cooling film of $u_2 = 0.1\,\mathrm{m\,s^{-1}}$ at $p = 1.013 \times 10^5$ Pa. At this condition the blowing ratio is $M_{CH_4} = 3.5$ for methane and $M_{H_2} = 0.27$ for hydrogen. The reference set-up is varied in temperature of the main stream ($T_\infty$), composition of the main stream ($\Phi$) and inlet velocity of the cooling film (varying the blowing ratio $M$).

### 3.3 Modelling

The flow field is solved as laminar flow with constant viscosity $\nu$; when the combustion model requires a turbulence model, then the $k$-$\epsilon$-model is chosen. Thermal diffusion is neglected and the Lewis number is set to unity. The combustion is first analyzed with a laminar finite-rate one step reaction. Then the equilibrium model and laminar non-premixed flamelet model are used. The flamelet tables are based on the GRI-3.0 detailed mechanism for methane. These analyses allow to evaluate the effects of different combustion models on film cooling simulations. Including a larger number of species and reaction-steps the computational costs increase but the chemical behaviour is better reproduced. Flamelet tables are built only for low strain rates because the flowfield is laminar due to the low Reynolds number and flame extinction will not occur. For the same reason the variance of mixture fraction cannot assume a value different from zero.

Non-premixed flamelet tables are generated with the chemistry solver Cosilab [13]. Here a 1-D counterflow laminar diffusion flame is solved. Two opposite axis-symmetric jets of fuel ($CH_4$ or $H_2$) at $T_2 = 300\,\mathrm{K}$ and oxidizer (hot air) at $T_\infty = 1800\,\mathrm{K}$ create a laminar diffusion flame stabilized at the location of stoichiometric mixture fraction. Equal diffusivity of the species is considered ($Le = 1$). The temperature and composition profiles in mixture fraction space are used to build tables, which are integrated by using a presumed $\beta$-PDF.

### 3.4 Validation

There are only few experimental results for cooling films with secondary reactions, therefore the numeric simulation is first validated against the analytical value of convective heat transfer coefficient for the reference set-up, using laminar boundary layer theory on a flat plate [14]:

$$Nu = 0.332 Re_x^{(1/2)} Pr^{(1/3)}. \tag{7}$$

The numerical simulation agrees well with the analytical values.

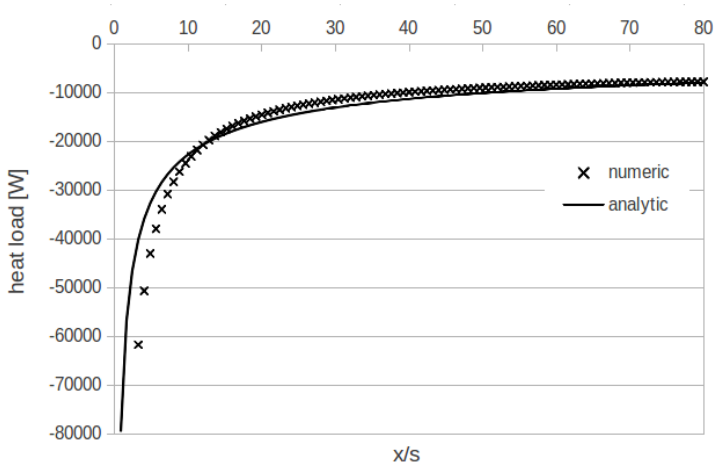


Figure 2: Comparison of numerical and analytical value for heat load over a flat plate

## 4. Results

### 4.1 Comparison of different combustion models

In this section different combustion models are compared. Figure 3a shows the temperature profiles in mixture fraction space for onestep reaction and full mechanism GRI-3.0 [15] for $CH_4$-air mixture. Using a onestep reaction, the maximum temperature is higher than with the full mechanism. Endothermic dissociation reactions take place in the real flow and the full mechanism is able to simulate this behaviour. The inflection in the full mechanism profile at rich conditions is a typical result for methane/air flames with equilibrium reaction [16]. This profile is obtained for very low strain rate, which means it is very close to equilibrium. The temperature is then the equilibrium temperature for each value of mixture fraction. In figure 3b different combustion models are compared for the reference set-up. The onestep mechanism for methane combustion in Fluent is taken from the Fluent material database; this mechanism was translated to the Chemkin Format for the flamelet generation and for OpenFOAM.
The mixing of the cooling film with the hot main stream gases, denoted by $\eta^\star$, for all models in Fluent is nearly identical. The results of the laminar finite rate model and the turbulent finite rate/ eddy dissipation model are identical. The turbulent combustion model switches from finite rate modelling to eddy dissipation when the turbulent mixing becomes faster than the combustion. Despite the use of a turbulence model the flow is still laminar and the turbulent mixing is therefore very small compared to the chemical reactions.
In OpenFOAM the cooling film mixes much faster with the main stream than in Fluent. This is probably caused by the different diffusion mechanism. Both solvers operate with a unity Lewis number, but the flow properties in OpenFOAM are not constant, but temperature dependent. The different mixing and therefore also different air-fuel ratio cause the faster increase of the temperature in the OpenFOAM simulation. The inflection point on the $\Theta$-graph for OpenFOAM

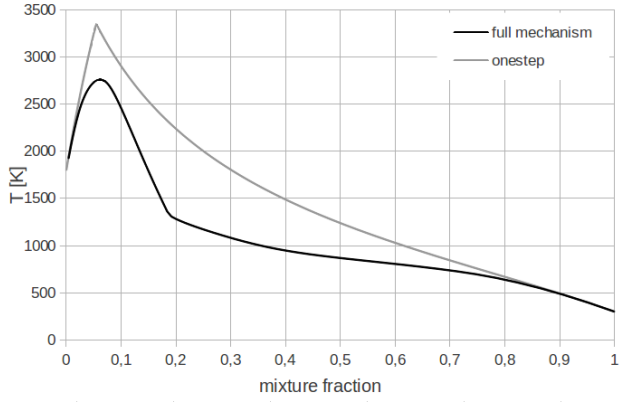


(a) Flamelet profiles for onestep $CH_4$ and GRI-3.0 mechanism

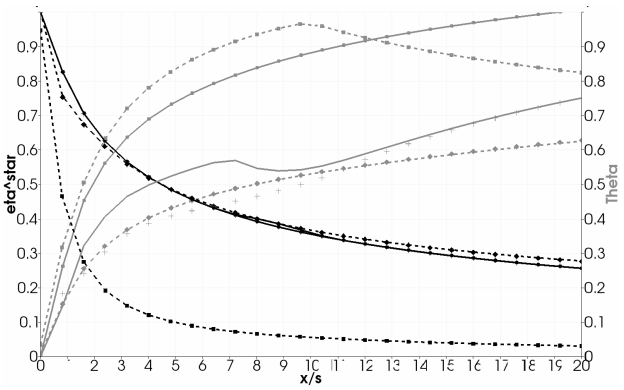


(b) *onestep mech.*: dashed line - finite rate, diamonds - finite rate/ eddy dissipation, line with circles - flamelet; dashed line with squares- OpenFOAM finite rate; *GRI-3.0*: plus - equilibrium, solid line - flamelet; black lines $\eta^\star$, grey lines $\Theta$

Figure 3: Comparison of different combustion models

is the result of the unsteady simulation in OpenFOAM. With this solver a steady-state simulation was not possible and the hot gases of the secondary reaction are not transported very far downstream.
Both combustion models using the GRI-3.0 mechanism agree well in $\Theta$ downstream, where equilibrium is reached. The bump of the temperature curve for the GRI-3.0 flamelet can also be seen in the flamelet profile in figure 3a. There is an inflection point in the temperature vs. mixture fraction curve at $Z \approx 0.2$, which translates to the bump in figure 3b at $x/s \approx 7$. The temperatures for the finite rate model (dashed line and diamonds in fig. 3b) is lower than for the flamelet models, because the mixture needs a certain ignition time, whereas in the flamelet model it is assumed that the combustion process is very fast. This mixed equals burned assumption is not able to predict ignition failure due to a mixture temperature below the ignition temperature or due to heat loss on a cooled wall.
The following results are obtained with the finite-rate model in Fluent, which is able to take the wall influence into account.

### 4.2 Influence of the temperature difference between main flow and film cooling

Starting from the reference set-up with $T_\infty = 1800\,\mathrm{K}$, the temperature of the main flow is gradually decreased to $T_\infty = 800\,\mathrm{K}$, until no chemical reactions between methane cooling film and air are observed. For the hydrogen cooling film the same temperature steps are chosen, although a hydrogen/air mixture ignites even at far lower temperatures. In figure 4 the results for both cooling gases on an adiabatic wall are plotted.

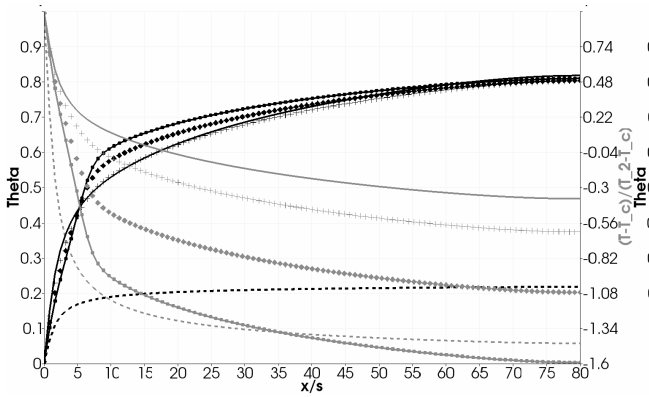


(a) $CH_4$, M=3.5

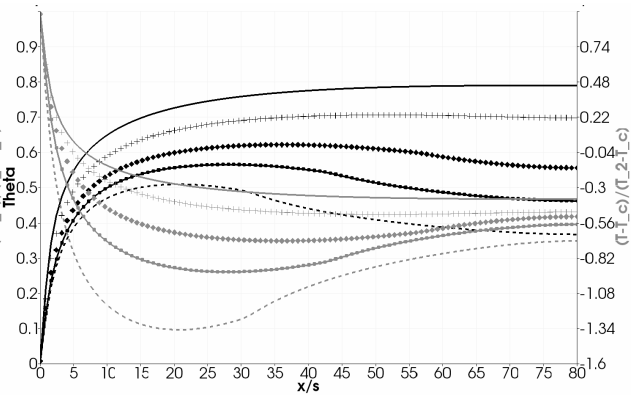


(b) $H_2$, M=0.27

Figure 4: Dimensionless wall temperature $\Theta$ (left scale, black) and the increase of wall temperature (right scale, grey) on an adiabatic wall; solid line: 1800 K, plus: 1500 K, diamonds: 1200 K, line with circles: 1000 K, dashed line: 800 K

The difference between a cooling film without reactions (for $CH_4$ $T_\infty = 800\,K$) and a cooling film with chemical reactions can be seen in figure 4a. The achieved wall temperature without reaction is much lower than with reaction. The value of $(T_w - T_\infty)/(T_2 - T_\infty)$, which equals the film cooling effectiveness for non reacting flows, can drop below zero, which means that the wall temperature $T_w$ is higher than the main stream temperature $T_\infty$. Therefore this definition of the film cooling effectiveness cannot be used. The effects of varying $T_\infty$ can be seen only close to the injection point. Far downstream of the cooling film injection the ratio of wall temperature to adiabatic flame temperature $\Theta$ varies only slightly. For a different cooling gas and different blowing ratio, this behaviour cannot be reproduced (see figure 4b). Whether this is an effect of the different diffusivity of the cooling film gases or of the blowing ratio will be examined in section 4.3. For the low blowing ratio in the $H_2$ cooling film case the mixing of the cooler main stream with the hot products can be seen to happen further downstream for higher main stream temperatures.
In figure 5 the detrimental effect of chemical reactions within the cooling film is shown via the increased heat load due to film cooling on a cooled wall ($T_w = 300\,K$). $T_\infty$ is only decreased to 1000 K, because for the cooled wall chemical reactions with the methane cooling film were only observed at temperatures higher than 1000 K. The cooled wall definitely influences the chemical reactions, which will also be discussed in section 4.3. Here the heat load

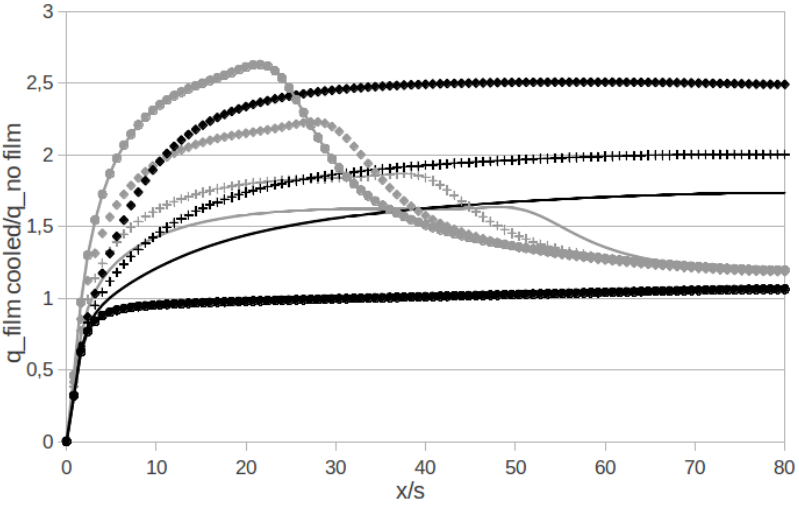


Figure 5: Ratio of heat load on film cooled wall to heat load on no-film cooled wall for different wall temperatures; black: $CH_4$, grey: $H_2$; solid line: 1800 K, plus: 1500 K, diamonds: 1200 K, line with circles: 1000 K

for the hydrogen cooling film far downstream the cooling slot is about 1.3 times higher than without film cooling, whereas for a methane cooling film the additional heat load due to film cooling depends more strongly on the main stream temperature. The question arises again, whether this is caused by the different blowing ratio or by the different diffusivity.

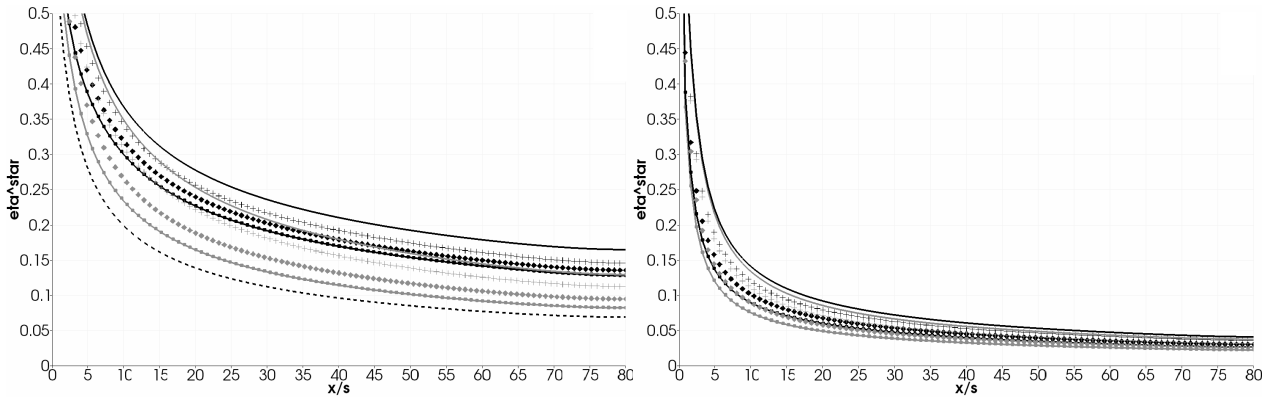


(a) $CH_4$ (b) $H_2$

Figure 6: Comparison of $\eta^\star$ for reacting cooling film (black) and non-reacting cooling film (grey) on adiabatic wall; solid line: 1800 K, plus: 1500 K, diamonds: 1200 K, line with circles: 1000 K, dashed line: 800 K

In figure 6 the film cooling effectiveness ($\eta^\star$, eq. (4)) is compared for cooling film with and without chemical reactions. For a reacting flow there is an increase of around 10% in the film cooling effectiveness for the hydrogen cooling film in comparison to a non reacting cooling film. The methane cooling film effectiveness $\eta^\star$ is increased by 30%. This increase is partly caused by the different flow fields due to the heat release, but also the hot reaction products seem to hinder the mixing of the cooling film with the main stream.
Empirical correlations of $\eta$ exist for different geometries for non-reacting cooling films. This simulation suggests a correlation in form of $\eta^\star = const \cdot \eta$ between the film cooling effectiveness $\eta^\star$ for a reacting cooling film and the effectiveness $\eta$ for the known non reacting film. But this needs to be investigated experimentally and/or with a more sophisticated approach on species diffusion and reaction mechanism.
Secondly a comparison of $\eta^\star$ for adiabatic wall and cooled wall (e.g. figure 7 or 10) shows slight discrepancy for the same set-up. This discrepancy can be explained by the different velocity fields due to the different temperature fields on the wall.

### 4.3 Influence of the blowing ratio

In figure 7 parameters of methane film cooling for different blowing ratios are plotted. For decreasing blowing ratio the film cooling effectiveness decreases and the wall temperature increases. The heat load at a cooled wall has a maximum near the injection and decreases afterwards for sufficiently low blowing ratios. The higher the blowing ratio, the less distinct is this maximum. To distinguish the different temperature characteristics between the methane and the hydrogen cooling film (shown in figure 5 and 6), a low blowing ratio methane cooling film was examined at a different temperature (cross symbol in figure 7). Like in figure 4b the temperature ratio $\Theta$ far downstream of the injection varies more for different temperatures at lower blowing ratios, and the heat flux for a cooled wall tends to a fixed value for different main stream temperatures (compare figure 5 and 7b). The different behaviour between methane and hydrogen cooling with respect to the main stream temperatures depends on the different blowing ratios.

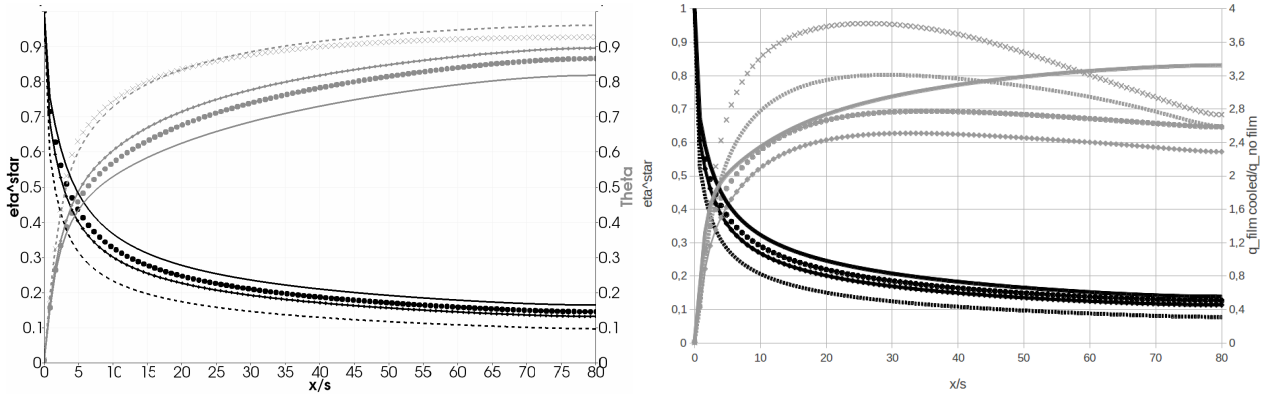


(a) adiabatic wall

(b) cooled wall

Figure 7: Parameters for methane cooling film for different blowing ratios; solid line: $M = 3.5$, circle: $M = 2.3$, line with diamonds: $M = 1.75$, dashed line: $M = 0.7$, cross: $T = 1500\,\mathrm{K}$ ; black lines: left axis, grey lines: right axis.

At lower blowing ratios the influence of the wall on the chemical reactions can be observed in figure 8.
The lower the blowing ratio, the nearer the chemical reactions take place to the wall. In figure 8 the profile of the heat release through the flame at $x/s = 1$ is plotted. On the adiabatic wall the heat release increases for lower blowing ratios because the mixing of the oxidizer rich main stream and the cooling film is further upstream. For the case of cooled wall, although nearly the same amount of oxidizer is available, the heat release is much lower compared to the adiabatic wall. Due to the enthalpy loss the flames are quenched. Evaluation of DNS data for premixed combustion from literature [17] shows that the wall influences the flame up to Peclet numbers of 10 and quenching occurs at around 3.5 flame brush thicknesses from the wall. The effect here is seen for a $y/s \approx 10$. Also the temperature, where reactions occur in a methane cooling film, rises with decreasing blowing ratio. When the blowing ratio is increased a former non-reacting cooling film can show secondary heat release due to chemical reactions, that are no longer quenched.

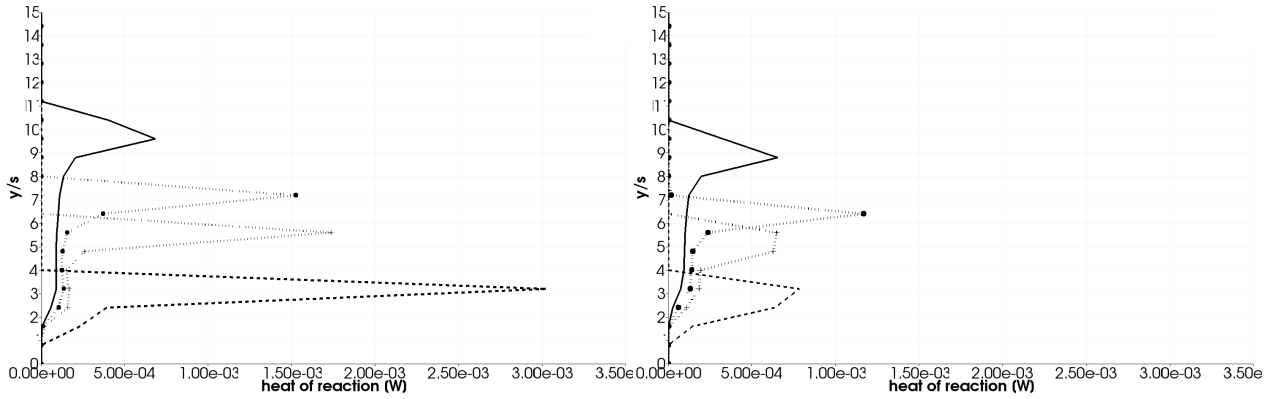


(a) adiabatic wall (b) cooled wall

Figure 8: Profile of heat of reaction at $x/s = 1$; solid line: $M = 3.5$, dotted line and circle: $M = 2.3$, dotted line and plus: $M = 1.75$, dashed line: $M = 0.7$

### 4.4 Influence of the main stream composition

A different main stream composition leads to different temperatures in the combustion chamber and to a different composition of the exhaust gases. For this investigation the main stream is assumed to be the exhaust gases from an ideal, adiabatic combustion process. Only lean mixtures are investigated, because for any chemical reactions to take place in the fuel cooling film, oxidizer must be present in the main stream. Rocket engines normally operate with rich overall mixtures, but still unburned pockets of oxidizer can be transported to the cooling film by large turbulent eddies. Within this simple study, these effects cannot be taken into account, therefore rich mixtures are omitted for now. For each equivilance ratio $\Phi$ not only the main stream composition, but the combustion temperature in the ideal combustor and therefore the main stream temperatures change, too.

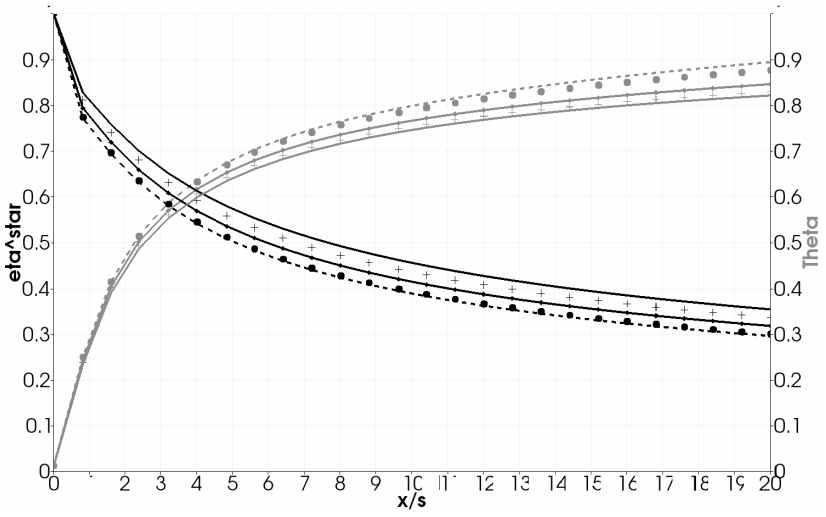


Figure 9: $\eta^\star$ (black) and $\Theta$ (grey) for different equivalence ratios in the main stream;
solid line: $\Phi = 1$, plus: $\Phi = 0.9$, solid line with diamonds: $\Phi = 0.8$, circles: $\Phi = 0.7$, dashed line: $\Phi = 0.6$

In figure 9 the film cooling effectiveness $\eta^\star$, as well as the temperature ratio $\Theta$ for different main stream compositions are shown. For increasing $\Phi$, which means less left-over oxidizer but higher main stream temperature, the film-cooling effectiveness increases and the temperature ratio decreases. Due to the really high main stream temperatures here, the detrimental effect of the secondary reactions in the cooling film are not so prominent as seen in the former sections with a hot air stream, but still the wall temperature and therefore the heat load are higher, when secondary reactions take place near the wall.

### 4.5 Influence of slot height

In this paragraph the effects of different slot heights are analyzed. By increasing the slot height, a thicker cooling film

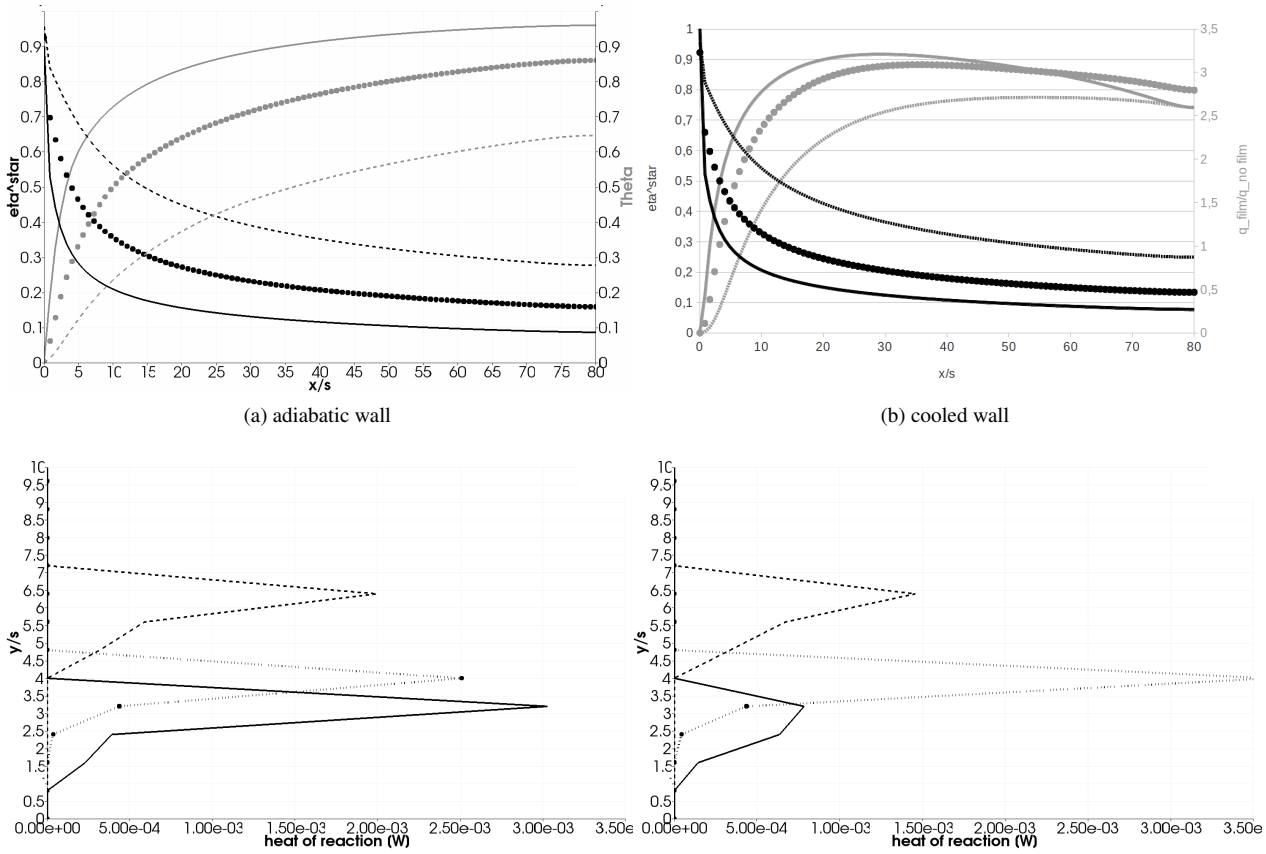


(a) adiabatic wall

(b) cooled wall

(c) adiabatic wall

(d) cooled wall

Figure 10: Parameters for methane cooling film for different slot heights;
solid line: $s = 0.25$ mm, circle: $s = 0.5$ mm, dashed line: $s = 1$ mm; black lines: left axis, grey lines: right axis

produces lower adiabatic wall temperature and the mixing of cooling film with the main stream takes longer (figures 10a and 10b). Secondly the chemical reactions due to mixing of main stream oxidizer and fuel cooling film take place further away from the wall (figures 10c and 10d), therefore the flames are not so strongly affected by the enthalpy loss. A thicker cooling film on the other hand needs more cooling mass flow, diminishing the engine efficiency and especially for the rocket application leading to bigger fuel tanks. It would reduce the heat load compared to the thin cooling film, but the heat load might still be higher than without film-cooling. A very thin cooling film would mean that the shear layer is within quenching distance of the wall and no additional heat release would occur. But then the film cooling effectiveness will be very low shortly after the injection and another injection would be necessary to protect the wall downstream. A trade-off between efficiency of film cooling and propulsion system weight has to be made in the engine design process.

## 5. Conclusion

When fuel and oxidizer mix in the cooling film, unwanted chemical reactions with additional heat release can occur. Using an inert gas cooling film is not practical because an additional tank with an inert gas needs to be carried, increasing the weight of the whole system. However, heat release in the cooling film is detrimental, so investigations on the occurrence of chemical reactions in the cooling film are necessary.
Due to the non-linearity of the energy equation for reactive flows, the well known parameter of film cooling effectiveness $\eta$ is not applicable anymore. We suggest a new definition for the film cooling effectiveness $\eta^\star$ based on a conserved scalar like the mixture fraction. To account for the heat release a temperature ratio $\Theta = (T_w - T_2)/(T_{ad,flame} - T_2)$ was

defined. The blowing ratio M is used to account for the influence from the flow fields of main stream and cooling film injection.
Most film-cooling applications operate in turbulent flow condition and use of a full combustion mechanism would be desirable to investigate the interaction of cooling film and reacting main stream. In a rocket combustion chamber most of the chemical reactions in the cooling film will be probably caused by pockets of oxidizer, which are transported via the turbulent motion to the wall. A full combustion mechanism with a finite rate chemistry mechanism leads to a very stiff set of additional equations, which are very time consuming and difficult to solve numerically. To circumvent this problem a flamelet model can be considered. The proximity to the wall influences the chemical reactions, which are slowed down or quenched due to enthalpy loss. This effects need to be considered and implemented in a flamelet model.
The wall, influencing the chemical reactions and heat release in the cooling film, makes the parameter $\Theta$ dependent on the boundary condition. The simulations show that the new film cooling effectiveness $\eta^\star$ for a reacting cooling cannot be predicted by known correlations for $\eta$ of a non-reactive cooling film, but a correlation between $\eta^\star$ and $\eta$ seems feasible. Even if oxidizer mixes with the fuel in the cooling film, the energy provided by the flow field may not be sufficient to ignite the mixture, when either the mixing temperature is too low or the mixing location is too close to the wall. Low main stream temperatures and a bigger quantity of oxidizer in the main stream increase the detrimental effect of the chemical reactions in the cooling film, raising the wall temperature to values higher than without film cooling.
Experimental data on reacting cooling films, especially for higher pressures, are required to better validate our results.

## Acknowledgments

Financial support for this work was provided by the DFG SFB-TR40 program.

## References

[1] Sutton, G. and O. Biblarz. 2001. Rocket Propulsion Elements. John Wiley & Sons, Inc. New York. 7.

[2] Dellimore, K. 2010. Modeling and Simulation of Mixing Layer Flows for Rocket Engine Film Cooling. PhD Thesis. University of Maryland. Department of Aerospace Engineering.

[3] Kirk, D., G. Guenette, S. Lukachko and I. Waitz. 2002. Gas Turbine Engine Durability Impacts of High-Fuel-Air Ratio Combustors Part 2: Near Wall Reaction Effects on Film-Cooled Heat Transfer. In: *Proceedings of ASME Turbo Expo.*

[4] Polanka, M., Zelina, J., Anderson, W. and B. Sekar. 2011. Heat Release in Turbine Cooling I: Experimental and Computational Comparison of Three Geometries. *J. of Propulsion and Power* 27:257-268.

[5] Lin, C., Holder, R., Sekar, B., Zelina, J., Polanka, M., Thornburg, H. and A. Briones. 2011. Impact of Heat Release in Turbine Cooling II: Numerical Details of Secondary Combustion Surrounding Shaped Holes. *J. of Propulsion and Power* 27:269-281.

[6] Liu, S., Fotache, C., Chao, B., Hautman, D. and S. Ochs. 2008. Boundary Layer Modeling of Reactive Flow over a Porous Surface with Angled Injection. *Combustion and Flame* 154:378-386.

[7] Arnold, R., Suslov, D., and O., Haidn. 2009. Experimental Investigation of Film Cooling with Tangential Slot Injection in a LOX/CH4 Subscale Rocket Combustion Chamber. *Transactions of Space Technology Japan* 7:81-86

[8] Arnold, R., Suslov, D., and O., Haidn. 2009. Circumferential Film Cooling Effectiveness in a LOX/H2 Subscale Combustion chamber. *J. of Propulsion and Power* 25:760-770.

[9] Arnold, R., Suslov, D., and O. Haidn. 2009. Film Cooling of Accelerated Flow in a Subscale Combustion Chamber. *J. of Propulsion and Power* 25:443-451.

[10] Lux, J., and O. Haidn. 2009. Flame Stabilization in High-Pressure Liquid Oxygen/Methane Rocket Engine Combustion. *J. of Propulsion and Power* 25:15-23.

[11] Goldstein, R. 1971. Film Cooling. In: *Advances in Heat Transfer.* 7:321-377.

[12] Celik, I., Ghia, U., Roache, P. and C. Freitas. 2008. Procedure for Estimation and Reporting of Uncertainty Due to Discretization in CFD Applications. *J. of Fluids Engineering* 130.

[13] COSILAB, Rotexo Software. Bochum 2012.

[14] Schlichting, H. and K. Gersten. 1997. Grenzschicht-Theorie. Springer Verlag. Berlin. 9.

[15] GRI-Mech 3.0. *www.me.berkeley.edugri_mech/version30/text30.html*.

[16] Peters, N.. 2004. Turbulent Combustion. Cambridge University Press.

[17] Poinsot, T., Harworth, D., and G. Bruneaux. 1993. Direct Numerical Simulation and Modeling of Flame-Wall Interaction for Premixed Combustion. *Combustion and Flame* 95:118-132.